Preprints of the 21st IFAC World Congress (Virtual)
Berlin, Germany, July 12-17, 2020

Second-Order SMC with Disturbance Compensation for Robust Tracking Control in PMSM Applications

Harald Aschemann * **Benedikt Haus** ** **Paolo Mercorelli** **

* *Chair of Mechatronics, University of Rostock, Justus-von-Liebig-Weg 6, D-18059 Rostock, Germany (e-mail: harald.aschemann@uni-rostock.de)*
** *Institute of Product and Process Innovation, Leuphana University of Lueneburg, Universitaetsallee 1, D-21335 Lueneburg, Germany (e-mail: haus@leuphana.de, mercorelli@uni.leuphana.de)*

Abstract: In this contribution, a cascaded control strategy is presented for a permanent magnet synchronous motor (PMSM) that compensates for model nonlinearities and enables an accurate as well as robust trajectory tracking. The proposed strategy comprises the combination of an inversion-based current control, one of two alternative second-order sliding mode control approaches (SMC) and an extended Kalman filter (EKF). The reference values for the inversion-based current controllers are calculated by a Maximum Torque Per Ampere (MTPA) strategy in an outer control loop. As second-order SMC approaches are investigated: one design based on an integrator extension of the control input, whereas the other is given by a hybrid twisting control. Both alternatives mitigate undesired chattering while the EKF yields smooth estimates for both the state variables and a lumped disturbance torque from noisy measurements. Moreover, the robustness of the overall control structure is increased, chattering effects are reduced and unknown disturbances as well as parameter uncertainty are addressed by combining second-order sliding mode control with estimator-based disturbance compensation. The potential of the proposed nonlinear control strategy is pointed out by successful simulation studies.

Keywords: PMSM, Extended Kalman Filter, Torque Control, Sliding Mode Control, Control Applications.

1. INTRODUCTION AND MOTIVATION

Due to their high power density, permanent magnet synchronous motors (PMSMs) are frequently used in applications with limited space for actuators. For this reason, they often have to be used in the high power region with large currents. As such a operation is related to several nonlinear effects, the choice of an appropriate control strategy is crucial and has a huge impact on the efficiency of these electrical machines. Control of PMSMs is a consolidated field of research, offering already many control strategies in different industrial branches. Most of them use linear approaches – like proportional-plus-integral (PI) and proportional-plus-integral-plus-derivative (PID) controllers – and nonlinear ones – like sliding mode control (SMC) as proposed in Zwerger and Mercorelli (2019), Zwerger and Mercorelli (2018). A reason for the popularity of SMC, see Y. Shtessel and Levant (2014), is the inherent robustness of SMC against parameter uncertainty, which is also beneficial for the control of the PMSM. One of the most crucial aspects to be addressed in SMC applications is the reduction of the chattering phenomenon. In this context, two alternative second-order schemes are adopted and compared to each other. In the field of PMSM control, the realization of a *sensorless control*, which intends to reduce the number of measured states and, hence, the number of sensors, is a challenging problem, cf. Bolognani et al. (1999). This reduction may be obtained using a state observer as a virtual sensor, see Mercorelli (2017), Mercorelli (2014) and Mercorelli (2015). For an effective sensorless control, an accurate system model is required, which poses problems in the case of model uncertainty. Recently, by means of an analytical sensitivity analysis, the contributions of Bolognani et al. (2018) and Soricellis et al. (2017) have addressed the influence of model uncertainty on the observed position and the robustness of a proportional-integral observer in the current control of PMSM drives. Aschemann et al. (2018) presented an integral sliding mode control in combination with a reduced-order disturbance observer for a permanent magnet linear actuator. In this paper, an innovative control approach of PMSM drives is presented. The main contributions are as follows:

- A combination of second-order SMC and an extended Kalman filter (EKF) for both state and disturbance estimation minimizes the tracking error even in the presence of disturbances and parameter uncertainty. Two alternative solutions are compared to each other.
- The EKF-based disturbance compensation enables a reduction of the switching height of the discontinuous control part and, consequently, a further reduction of the chattering phenomenon is obtained. Moreover,

also the impact of parameter uncertainty on the motor torque can be counteracted efficiently.
- In the underlying inversion-based current control, the estimated rotor velocity is employed for a model-based compensation of the induced voltage.

The given paper is structured as follows: In Sect. 2, the physical system modelling of the PMSM is described briefly. Sect. 3 deals with the cascaded nonlinear control design. Here, Subsect. 3.1 presents an inversion-based current control to determine the desired input voltages $u_d(t)$ and $u_q(t)$ of a d/q-model of the PMSM. The desired currents $i_d(t)$ and $i_q(t)$ are calculated by means of the well-known maximal torque per Ampere (MTPA) method, as described in Subsect. 3.2. The desired torque is determined using second-order sliding mode control (SOSMC) – either a variant based on an integrator extension of the input or a hybrid twisting controller –, see Sect. 3.3. In particular, SOSMC counteracts model uncertainty and external disturbances and, hence, guarantees the robustness of the control strategy. Both the state variables and a lumped disturbance are estimated by an extended Kalman filter (EKF) presented in Sect. 4. They are employed subsequently for compensation purposes. Thereby, the SMC is relieved and undesired chattering is reduced. Simulation results in Sect. 5 indicate tracking accuracy even in the presence of unknown disturbances. Finally, the paper closes with conclusions.

2. DYNAMIC MODELLING OF THE PMSM

The two-axis dq-model of the PMSM, obtained by using Park's dq-transformation, is the most widely used among a variety of models in the literature, especially for variable-speed control applications, see M.A. Rahman and King-Jet (2003) and Khaburi and Shahnazari (2003). Park's dq-transformation represents a nonlinear coordinate transformation that converts the three-phase stationary variables into variables of a rotating coordinate system. A PMSM with interior magnets is subject to saturation and cross coupling effects, where both are load-dependent. The flux linkages

$$\begin{aligned} \psi_d(t) &= L_d(i_d(t))i_d(t) + \psi_p \ , \\ \psi_q(t) &= L_q(i_q(t))i_q(t) \end{aligned} \tag{1}$$

act simultaneously and interfere within the stator. In this paper, cross couplings and saturation effects are not included in the model, and linear equations employed for the flux linkage. Nevertheless, the impact of parameter uncertainty on the motor torque is counteracted by disturbance estimation and compensation. The permanent flux acts in the same direction as ψ_d. The permanent magnetic flux from the rotor over the air gap and the stator is denoted by ψ_p. The other portion of magnetic flux which is present in the rotor is not considered in ψ_p. The voltage balances result in

$$\begin{aligned} u_d(t) &= L_d\frac{\mathrm{d}i_d(t)}{\mathrm{d}t} + R_s i_d(t) - L_q p\omega_r(t) i_q(t) \ , \\ u_q(t) &= L_q\frac{\mathrm{d}i_q(t)}{\mathrm{d}t} + R_s i_q(t) + L_d p\omega_r(t) i_d(t) + \psi_p p\ \omega_r(t) \ . \end{aligned} \tag{2}$$

These equations can be stated in a compact matrix-vector form as follows

$$\begin{aligned} \underbrace{\begin{bmatrix} u_d(t) \\ u_q(t) \end{bmatrix}}_{\mathbf{u}(t)} &= \underbrace{\begin{bmatrix} -L_q p\omega_r(t) i_q(t) \\ L_d p\omega_r(t) i_d(t) + \psi_p p\omega_r(t) \end{bmatrix}}_{\mathbf{u}_p(t)} \\ &+ \underbrace{\begin{bmatrix} L_d & 0 \\ 0 & L_q \end{bmatrix}}_{\mathbf{L}} \underbrace{\begin{bmatrix} \frac{\mathrm{d}i_d(t)}{\mathrm{d}t} \\ \frac{\mathrm{d}i_q(t)}{\mathrm{d}t} \end{bmatrix}}_{\frac{\mathrm{d}\mathbf{i}(t)}{\mathrm{d}t}} + \underbrace{\begin{bmatrix} R_s & 0 \\ 0 & R_s \end{bmatrix}}_{\mathbf{R}} \underbrace{\begin{bmatrix} i_d(t) \\ i_q(t) \end{bmatrix}}_{\mathbf{i}(t)} \end{aligned} \tag{3}$$

Here, $i_d(t)$, $i_q(t)$, $u_d(t)$ and $u_q(t)$ are the dq-components of the stator currents and voltages in a synchronously rotating rotor-fixed reference frame, and $\omega_r(t)$ is the rotor angular velocity. Given the number of permanent magnet pole pairs p, the electrical angular velocity becomes $\omega_{el}(t) = p\omega_r(t)$. The other system parameters R_s, L_d, and L_q stand for the stator resistance and the inductances of the d-axis and q-axis, respectively. The dynamic electrical model of the synchronous motor in dq-coordinates can now be stated in state-space form

$$\begin{aligned} \begin{bmatrix} \frac{\mathrm{d}i_d(t)}{\mathrm{d}t} \\ \frac{\mathrm{d}i_q(t)}{\mathrm{d}t} \end{bmatrix} &= \underbrace{\begin{bmatrix} -\frac{R_s}{L_d} & -\frac{L_q p\omega_r(t)}{L_d} \\ \frac{L_d p\omega_r(t)}{L_q} & -\frac{R_s}{L_q} \end{bmatrix}}_{\mathbf{A}} \underbrace{\begin{bmatrix} i_d(t) \\ i_q(t) \end{bmatrix}}_{\mathbf{i}(t)} + \\ &\underbrace{\begin{bmatrix} \frac{1}{L_d} & 0 \\ 0 & \frac{1}{L_q} \end{bmatrix}}_{\mathbf{B}} \left\{ \underbrace{\begin{bmatrix} u_d(t) \\ u_q(t) \end{bmatrix}}_{\mathbf{u}(t)} - \underbrace{\begin{bmatrix} 0 \\ \psi_p p\omega_r(t) \end{bmatrix}}_{\mathbf{e}_p(t)} \right\} \ , \end{aligned} \tag{4}$$

with the induced voltage vector $\mathbf{e}_p(t)$. The motor torque, which represents the controlled output, is given by

$$M_M(t) = \frac{3}{2}p\Big\{ i_q(t)\psi_d(t) - i_d(t)\psi_q(t) \Big\}, \tag{5}$$

where the term $(i_q(t)\psi_d(t) - i_d(t)\psi_q(t))$ defines the cross coupling within the PMSM dynamics, which also leads to the effect that a variation of the current $i_d(t)$ has an impact on the current $i_q(t)$ in the q-axis and vice versa. By introducing the inductances according to (1), the torque can be expressed alternatively in the form

$$M_M(t) = \frac{3}{2}p\Big\{ (L_d - L_q)i_d(t)i_q(t) + \psi_p i_q(t) \Big\}. \tag{6}$$

This drive torque affects the angular velocity of the rotor described by the mechanical equation of motion

$$J\frac{\mathrm{d}\omega_r(t)}{\mathrm{d}t} = M_M(t) - d\omega_r(t) - M_0(t) \ . \tag{7}$$

In addition to viscous damping, characterized by the coefficient d, a lumped disturbance torque $M_0(t)$ – accounting for nonlinear friction, an external load torque and the impact of parameter uncertainty – are considered. J represents the mass moment of inertia of the rotor.

3. CONTROL STRUCTURE

Starting from the outer loop, the structure of the control strategy consists of a combination of an external second-order SMC and an internal MTPA module that calculates optimal currents, see the block diagram in Fig. 1. In the inner loop, an inversion-based current control (IBCC) is

employed that generates the desired input voltages. An EKF is applied to reconstruct the states of the system and in particular to estimate an unknown lumped disturbance torque acting on the rotor.

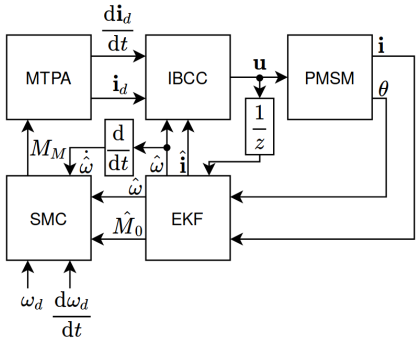

Fig. 1. Block diagram of the overall control structure.

3.1 Inversion-Based Current Control

For the current control, an inversion-based design is suitable and allows for a linear first-order error dynamics. For this purpose, the right-hand side should be equal to the sum of the time derivatives $d(\mathbf{i}_d(t))/dt$ of the desired currents and a feedback term given by the product of a diagonal matrix $\mathbf{\Lambda} = \mathrm{diag}[\lambda, \lambda]$ and the tracking error $\mathbf{i}_d(t) - \mathbf{i}(t)$. This results directly in

$$\begin{aligned}\frac{d\mathbf{i}(t)}{dt} &= \mathbf{A}\ \mathbf{i}(t) + \mathbf{B}\left[\mathbf{u}(t) - \hat{\mathbf{e}}_p(t)\right] \\ &= \frac{d\mathbf{i}_d(t)}{dt} + \mathbf{\Lambda}[\mathbf{i}_d(t) - \mathbf{i}(t)]. \end{aligned} \tag{8}$$

Equation (8) can be solved for the desired input vector $\mathbf{u}(t)$, which results in

$$\mathbf{u}(t) = \mathbf{L}\left[\frac{d\mathbf{i}_d(t)}{dt} + \mathbf{\Lambda}[\mathbf{i}_d(t) - \mathbf{i}(t)]\right] + \mathbf{R}\ \mathbf{i}(t) + \hat{\mathbf{e}}_p(t). \tag{9}$$

To compensate for the induced voltages in the current dynamics, a model-based estimate $\hat{\mathbf{e}}_p(t)$ is determined according to (4) – evaluated with the estimated rotor angular velocity $\hat{\omega}_r(t)$ provided by the EKF.

3.2 Maximum Torque Per Ampere (MTPA)

The losses in the machine depend on the copper losses and increase quadratically with the machine currents. Given the desired motor torque $M_M(t)$, the MTPA method provides optimal values for the desired dq-currents $i_{dd}(t)$ and $i_{qd}(t)$. These currents are subsequently used as reference inputs in the inner loop of the cascaded control structure. The aim of maximizing the motor torque with minimal dq-currents leads to a equality-constrained optimization problem, which can be addressed symbolically by an augmented Lagrangian. The torque determined in the outer control loop for the angular velocity represents the desired torque

$$M_d(t) = M_M(t) = \frac{3}{2}p[i_q(t)\psi_p + (L_d - L_q)i_d(t)i_q(t)]\ , \tag{10}$$

that should be realized with the smallest currents possible and in compliance with a side condition for the currents

$$i(t) = \sqrt{i_d^2(t) + i_q^2(t)}\ \rightarrow\ i^2(t) - i_d^2(t) - i_q^2(t) = 0 \tag{11}$$

The Lagrangian is then

$$\begin{aligned}\mathcal{L} = -\frac{3}{2}p[i_q(t)\psi_p + (L_d - L_q)i_d(t)i_q(t)] \\ + \lambda(i^2(t) - i_d^2(t) - i_q^2(t)),\end{aligned} \tag{12}$$

where λ is a Lagrange multiplicator for the side condition. The necessary optimality condition is given by vanishing first partial derivatives with respect to $i_q(t), i_d(t)$, and $\lambda(t)$. In addition to (11), this leads to

$$\frac{\partial\mathcal{L}}{\partial i_q(t)} = -\frac{3}{2}p[\psi_p + (L_d - L_q)i_d(t)] - 2\lambda i_q(t), \tag{13}$$

$$\frac{\partial\mathcal{L}}{\partial i_d(t)} = -\frac{3}{2}p[i_q(t)(L_d - L_q)] - 2\lambda i_d(t). \tag{14}$$

Equations (13) and (14) are set to zero and solved to find the optimal solutions for $i_d(t)$ and $i_q(t)$

$$i_{d_{1/2}}(t) = -\frac{\psi_p}{2(L_d - L_q)} \pm \frac{1}{2}\sqrt{\left(\frac{\psi_p}{L_d - L_q}\right)^2 + 4i_q^2(t)}. \tag{15}$$

For a local minimum, the second derivatives are required to show the positive definiteness of the Hessian. They become

$$\frac{\partial^2\mathcal{L}}{\partial i_q^2(t)} = \frac{\partial^2\mathcal{L}}{\partial i_d^2(t)} = -2\lambda(t), \tag{16}$$

$$\frac{\partial^2\mathcal{L}}{\partial i_d(t)\partial i_q(t)} = -\frac{3}{2}p[L_d - L_q]. \tag{17}$$

A positive definite Hessian is obtained if λ is chosen negative. Then, the currents $i_{d_{1/2}}(t)$ of (15) have to be inserted in the solution for (13) or (14). If $L_d \neq L_q$ holds, e.g. in the case of an anisotropic machine and, especially $L_d < L_q$, then the current $i_d(t)$ follows for any given current $i_q(t)$ ($i_q(t) > 0$ for motor mode and $i_q(t) < 0$ for generator mode) as

$$i_d(t) = -\frac{\psi_p}{2(L_d - L_q)} - \frac{1}{2}\sqrt{\left(\frac{\psi_p}{L_d - L_q}\right)^2 + 4i_q^2(t)}. \tag{18}$$

3.3 Second-Order Sliding Mode Tracking Control

In this section, two alternative solutions for a second-order SMC are discussed for a tracking control of the angular velocity $\omega_r(t)$.

Asymptotic Second-Order SMC (SOSMC) For the design of the tracking control, the equation of motion (7) for the rotor is stated in state-space form and extended by an integrator at the input according to

$$\frac{d}{dt}\begin{bmatrix}\omega_r(t)\\ M_M(t)\end{bmatrix} = \begin{bmatrix}\dfrac{M_M(t) - d\omega_r(t) - M_0(t)}{J}\\ u(t)\end{bmatrix}. \tag{19}$$

Here, $u(t) = \dot{M}_M(t)$ represents the new control input. To simplify the notation, the time argument is omitted in the following derivation. For the second-order sliding mode control, a classical integral sliding surface is defined

$$s = \dot{\tilde{\omega}}_r + \alpha_0\tilde{\omega}_r + \alpha_I\int_0^t \tilde{\omega}_r d\tau,$$

where $\tilde{\omega}_r = \omega_d - \omega_r$ denotes the tracking error w.r.t. the angular velocity. The coefficients $\alpha_0 > 0$ and $\alpha_I > 0$ are chosen as positive values. Here, steady-state accuracy is guaranteed by the integral part, which also contributes to

the robustness of the position tracking. Accordingly, the first time derivative $\dot{s}$ becomes

$$\dot{s} = \ddot{\tilde{\omega}}_r + \alpha_0 \dot{\tilde{\omega}}_r + \alpha_I \tilde{\omega}_r. \tag{20}$$

Then, a quadratic Lyapunov function

$$V(s) = \frac{1}{2} s^2 \tag{21}$$

is introduced and the corresponding reaching condition is chosen

$$\dot{V}(s, \dot{s}) = s\dot{s} \leq -\eta \, |s| = -\eta \; s \; \mathrm{sign}(s). \tag{22}$$

With the choice $\tilde{\eta} > \eta > 0$, which corresponds to a slightly increased switching height, and the first time derivative of (20), the reaching condition results in

$$\ddot{\omega}_{rd} - \underbrace{\ddot{\omega}_r}_{\upsilon} + \alpha_0 \dot{\tilde{\omega}}_r + \alpha_I \tilde{\omega}_r = -\tilde{\eta} \; \mathrm{sign}(s). \tag{23}$$

Here, the highest derivative is chosen as a stabilizing control input, i.e., $\ddot{\omega}_r = \upsilon$. The corresponding stabilizing control law follows as

$$\upsilon = \ddot{\omega}_{rd} + \alpha_0 \dot{\tilde{\omega}}_r + \alpha_I \tilde{\omega}_r + \tilde{\eta} \; \mathrm{sign}(s). \tag{24}$$

A useful measure towards a further reduction of chattering is given by a regularisation of the switching part according to

$$\upsilon = \ddot{\omega}_{rd} + \alpha_0 \dot{\tilde{\omega}}_r + \alpha_I \tilde{\omega}_r + \tilde{\eta} \; \tanh\left(\frac{s}{\epsilon}\right). \tag{25}$$

As a result, however, a perfect sliding mode, see Slotine and Li (1991), is no longer possible. Instead, a real sliding mode occurs characterized by a small boundary layer around $s = 0$ with a thickness determined by a small parameter ϵ. The time derivative of desired motor torque

$$\dot{M}_M(t) = J\upsilon + d\dot{\omega}_r(t) + \dot{\hat{M}}_0(t) \tag{26}$$

follows from inserting this control law into the time derivative of the equation of motion for the rotor. Here, however, the time derivative of the disturbance estimate $\hat{M}_0(t)$ provided by the EKF would be needed. Note that the switching control parts does not affect the drive torque but its time derivative. For the implementation, the continuous part is integrated beforehand – which avoids a differentiation of the disturbance estimate according to

$$M_M(t) = J\left[\dot{\omega}_{rd}(t) + \alpha_0 \tilde{\omega}_r(t)\right] + d\omega_r + \hat{M}_0(t) \tag{27}$$

$$+ \int_0^t \left[J\alpha_I \tilde{\omega}_r(\tau) + \tilde{\eta} \; \tanh\left(\frac{s(\tau)}{\epsilon}\right)\right] d\tau. \tag{28}$$

Hybrid Twisting SMC (HTSMC) As an alternative higher-order sliding mode control approach the hybrid twisting algorithm is discussed, which is based on both the twisting as well as the super-twisting algorithms, see Friedland (1996) and Levant and Pridor (2000). For this purpose, a modified sliding surface is employed for the equation of motion (7) according to

$$s(t) = \tilde{\omega}_r(t) + \alpha_I \int_0^t \tilde{\omega}_r(\tau) d\tau,$$

which allows for computing the equivalent control $M_{M,eq}(t)$ by setting $\dot{s} = 0$ according to

$$M_{M,eq}(t) = J\left[\dot{\omega}_{rd}(t) + \alpha_I \tilde{\omega}_r(t)\right] + d\omega_r(t) + \hat{M}_0(t). \tag{29}$$

The inverse dynamics results in

$$M_M(t) = M_{M,eq}(t) - J\nu, \tag{30}$$

where ν represents an additional term that is determined by one of the three twisting algorithms presented subsequently.

Twisting Algorithm The basic twisting algorithm corresponds to the control law

$$\dot{\nu} = \begin{cases} -\nu, & |\nu| > 1 \\ -\alpha_m \mathrm{sign}(s), & s\dot{s} \leq 0, \;\; |\nu| \leq 1 \\ -\alpha_M \mathrm{sign}(s), & s\dot{s} > 0, \;\; |\nu| \leq 1 \end{cases}, \tag{31}$$

where the parameters α_M and α_m satisfy the conditions

$$\begin{aligned} &\alpha_M > \alpha_m \; , \quad \alpha_m > \tfrac{4\Gamma_M}{s_0} \; , \quad \alpha_M > \tfrac{\Phi}{\Gamma_m} \; , \\ &\Gamma_m \alpha_M - \Phi > \Gamma_M \alpha_m + \Phi \; . \end{aligned} \tag{32}$$

Super-Twisting Algorithm The super-twisting algorithm comprises the combined control law

$$\begin{aligned} \nu_{i,2} &= \begin{cases} -\lambda \, |s_0|^\rho \, \mathrm{sign}(s_i), & |s_i| > s_0 \\ -\lambda \, |s_i|^\rho \, \mathrm{sign}(s_i), & |s_i| \leq s_0 \end{cases}, \\ \dot{\nu}_{i,1} &= \begin{cases} -\nu_i, & |\nu_i| > 1 \\ -W \mathrm{sign}(s_i), & |\nu_i| \leq 1 \end{cases}, \\ \nu_i &= \nu_{i,1} + \nu_{i,2} \; , \end{aligned} \tag{33}$$

with the corresponding sufficient conditions for the control design parameters W, λ and ρ

$$W > \tfrac{\Phi}{\Gamma_m} \; , \quad \lambda^2 \geq \tfrac{4\Phi\Gamma_M(W+\Phi)}{\Gamma_m^3(W-\Phi)} \; , \quad 0 < \rho \leq 0.5 \; . \tag{34}$$

In the case of $|s| < s_0$, the positive constants Γ_m and Γ_M represent the lower and upper bounds of the total time derivative $\dot{s}$, whereas the variable Φ denotes the upper bound of the second time derivative $\ddot{s}$, see Levant and Pridor (2000) for more details.

Hybrid Twisting Algorithm In this paper, a hybrid controller is employed that combines the twisting and the super-twisting algorithm. It offers a high robustness and a faster convergence rate in comparison to the SMC controllers (31) and (33), see Levant and Pridor (2000). The hybrid twisting sliding mode control (HTSMC) is described by

$$\begin{aligned} \nu_2 &= \begin{cases} -\lambda \, |s_0|^\rho \, \mathrm{sign}(s), & |s| > s_0 \\ -\lambda \, |s|^\rho \, \mathrm{sign}(s), & |s| \leq s_0 \end{cases}, \\ \dot{\nu}_1 &= \begin{cases} -\nu, & |\nu| > 1 \\ -\alpha_m \mathrm{sign}(s), & s\dot{s} \leq 0, \;\; |\nu| \leq 1 \\ -\alpha_M \mathrm{sign}(s), & s\dot{s} > 0, \;\; |\nu| \leq 1 \end{cases}, \\ \nu_i &= \nu_1 + \nu_2 \; . \end{aligned} \tag{35}$$

For a further reduction of high frequency chattering the switching function $\mathrm{sign}(s)$ can be replaced by the smooth function $\tanh\left(\frac{s}{\epsilon}\right)$, $\epsilon > 0$.

4. COMBINED STATE AND DISTURBANCE ESTIMATION

In the given application, only selected measurements are available to implement the nonlinear control structure: the rotor angle $\theta_r(t)$ and well as the currents $i_d(t)$ and $i_q(t)$. Unfortunately, all these measurements are affected by errors like deterministic offsets and stochastic disturbances, e.g. white noise processes. Given the nonlinear system model, a discrete-time extended Kalman filter (EKF) can be advantageously employed and provides estimates with minimum covariances. The typical design is based on uncorrelated process noise and measurement noise that are assumed to be Gaussian, white and with a zero mean value. Despite the fact that in practice these assumptions

may not be completely true, the estimator usually provides meaningful state and disturbance estimates.

The design of the EKF is based on the dynamics of the dq-currents, the equation of motion for the rotor and, in addition, an integrator disturbance model $\dot{M}_0(t) = 0$ for the unknown disturbance torque $M_0(t)$. The extended state-space representation becomes

$$\begin{aligned} \mathbf{x}_{KF}(t) &= [i_d(t)\ i_q(t)\ \theta_r(t)\ \omega_r(t)\ M_0(t)]^T, \\ \dot{\mathbf{x}}_{KF}(t) &= \mathbf{f}_{KF}(\mathbf{x}_{KF}(t)) + \mathbf{B}_{KF}\mathbf{u}_{in}(t), \end{aligned} \tag{36}$$

$$\underbrace{\begin{bmatrix} \dfrac{-R_s}{L_d} i_d(t) + \dfrac{L_q p \omega_r}{L_d} i_q(t) \\ \dfrac{-L_d p}{L_q}\omega_r(t) i_d(t) - \dfrac{R_s}{L_q} i_q(t) - \dfrac{\psi_p p}{L_q}\omega_r(t) \\ \omega_r(t) \\ \dfrac{3p}{2J}[(L_d - L_q) i_q(t) i_d(t) + \psi_p i_q(t)] - \dfrac{d}{J}\omega_r(t) - \dfrac{1}{J} M_0(t) \\ 0 \end{bmatrix}}_{\mathbf{f}_{KF}(\mathbf{x}_{KF}(t))}$$

$$\mathbf{B}_{KF} = \begin{bmatrix} \dfrac{1}{L_d} & 0 & 0 & 0 & 0 \\ 0 & \dfrac{1}{L_q} & 0 & 0 & 0 \end{bmatrix}^T, \tag{37}$$

with inputs $\mathbf{u}_{in}(t) = [u_d(t)\ u_q(t)]^T$. The disturbance torque $M_0(t)$ is estimated as well to compensate for it in the cascaded controller and corresponds to zero element in the vector $\mathbf{f}_{KF}(\mathbf{x}_{KF}(t))$, which is evaluated in each time step with the last estimate. The corresponding model uncertainty is addressed by a large diagonal entry in the covariance matrix $\mathbf{Q}_{KF}$.

In the prediction step of the EKF algorithm, the a-priori estimates are calculated according to

$$\hat{\mathbf{x}}^-_{KF}(k+1) = \hat{\mathbf{x}}^+_{KF}(k) + T_s \mathbf{f}_{KF}(\hat{\mathbf{x}}^+_{KF}(k)) + T_s \mathbf{B}_{KF}\mathbf{u}_{in}(k), \tag{38}$$

which is the result of an explicit Euler discretisation with the sampling time T_s. For the first step, initial values $\hat{\mathbf{x}}^+_{KF}(0)$ can be either specified by the user or simply set to zero. The same applies to the initial uncertainty $\mathbf{P}^+(0)$ in the following equation. With the Jacobian $\mathbf{A}_{KF,d}$, the a-priori estimate of the covariance matrix is

$$\mathbf{P}^-(k+1) = \mathbf{A}_{KF,d}\mathbf{P}^+(k)\mathbf{A}^T_{KF,d} + \mathbf{Q}_{KF}, \tag{39}$$

where $\mathbf{Q}_{KF}$ represents a $\mathbb{R}^{5\times5}$ matrix quantifying the covariance matrix of the process noise. The Kalman gain can now be calculated as

$$\mathbf{K}(k+1) = \mathbf{P}^-(k+1)\mathbf{C}^T(\mathbf{C}\mathbf{P}^-(k+1)\mathbf{C}^T + \mathbf{R}_{KF})^{-1}, \tag{40}$$

with the measurement matrix $\mathbf{C}$ according to $\mathbf{x}_m(t) = \mathbf{C}\mathbf{x}_{KF}(t)$. Here, the vector $\mathbf{x}_m(t) = [i_d(t)\ i_q(t)\ \theta_r(t)]^T$ characterises the measured states, and the measurement covariance matrix $\mathbf{R}_{KF}$ is chosen a diagonal matrix

$$\mathbf{C} = \begin{bmatrix} 1 & 0 & 0 & 0 & 0 \\ 0 & 1 & 0 & 0 & 0 \\ 0 & 0 & 1 & 0 & 0 \end{bmatrix}, \ \mathbf{R}_{KF} = \begin{bmatrix} r_{i_1} & 0 & 0 \\ 0 & r_{i_2} & 0 \\ 0 & 0 & r_x \end{bmatrix}. \tag{41}$$

In the correction step of the Kalman filter algorithm, the a-posteriori estimates for covariance and states become

$$\mathbf{P}^+(k+1) = (\mathrm{I}_{5\times5} - \mathbf{K}(k+1)\mathbf{C})\,\mathbf{P}^-(k+1), \tag{42}$$

$$\hat{\mathbf{x}}^+_{KF}(k+1) = \hat{\mathbf{x}}^-_{KF}(k+1) + \Delta\mathbf{x}_{KF}(k+1), \tag{43}$$

where the correction term $\Delta\mathbf{x}_{KF}(k+1)$ is weighted by the Kalman gain $\mathbf{K}(k+1)$

$$\Delta\mathbf{x}_{KF}(k+1) = \mathbf{K}(k+1)\left(\mathbf{x}_m(k+1) - \mathbf{C}\hat{\mathbf{x}}^-_{KF}(k+1)\right). \tag{44}$$

The estimated states are used in the cascaded control design.

Apart from velocity-proportional damping, a repeated pulse-like load torque $M_L(t)$ with an amplitude of 0.5 Nm is employed in addition to a LuGre friction torque $M_{LuGre}(t)$ in the simulation model. The simplified LuGre model is given in a well-known standard form

$$\dot{z}(t) = \omega_r(t) - \sigma_0 z(t)\frac{|\omega_r(t)|}{M_c + (M_s - M_c)e^{-\left(\frac{\omega_r(t)}{\omega_s}\right)^2}}, \tag{45}$$

$$M_{LuGre}(t) = \sigma_0 z(t) + \sigma_1 \dot{z}(t) + \sigma_2 \omega_r(t). \tag{46}$$

Its parameters are described in detail, for example, in Åström and de Wit (2008). The LuGre friction model involves an additional state variable $z(t)$, which can be interpreted as the deflection of a stiff virtual bristle. For feedback control purposes, the EKF described in Sect. 4 is used to determine the estimate $\hat{M}_0(t)$ for the lumped disturbance torque that may comprise nonlinear friction, an external disturbance torque and the impact of parameter uncertainty on the motor torque. The torque requested from MTPA has to be increased accordingly by the estimated disturbance torque to achieve an accurate tracking of the angular velocity.

5. SIMULATION RESULTS

The simulation scenario focusses on the tracking of a polynomial change of the angular velocity from 0 rad/s to 100 rad/s in 0.2 sec, see Fig. 2. For the simulation study, the control and estimation algorithms were implemented in Simulink, while the PMSM was simulated – with and without parameter uncertainty – using the system model presented in Sec. 2. Note that this model is standard in the control-oriented literature and corresponds to the Simscape block supplied with the Simscape Electrical toolbox by MathWorks. Overall, the following 16 combinations are considered and compared to each other:

- SOSMC or HTSMC as control approaches
- two different initial conditions: $\omega_r(0) = 5$ rad/sec or $\omega_r(0) = 0$ rad/sec
- with or without disturbance compensation (DC)
- with or without parameter uncertainty in the inductances: L_q is enlarged by 40 %, whereas L_d is reduced by 40 %

The numerical values for the root-mean-squared error (RMSE) are stated in SI units in Table 1. Obviously, both approaches perform almost similarly well.

5.1 Simulation Results Without Parameter Uncertainty

In the sequel, the controllers employ the same inductances as in the PMSM simulation model. In Fig. 2, a comparison of desired and simulated values are presented for both SOSMC and HTSMC. As they could almost not be differentiated from the desired ones, the corresponding tracking errors are depicted in Fig. 3. In the case without parameter uncertainty, the estimate for the lumped disturbance corresponds to the sum of nonlinear friction as well as the external disturbance torque, see Fig. 4. The

Table 1. Performance of the SMC variants

Controller variant	SOSMC				HTSMC			
Parameter error	✓		✗		✓		✗	
Disturbance compensation	✓	✗	✓	✗	✓	✗	✓	✗
RMSE $\omega_r(0) = 5$	0.1417	0.1419	0.1407	0.1407	0.1554	0.1555	0.1566	0.1566
RMSE $\times 10^{-3}$ $\omega_r(0) = 0$	11.72	14.51	0.869	1.063	11.47	13.14	0.685	0.830

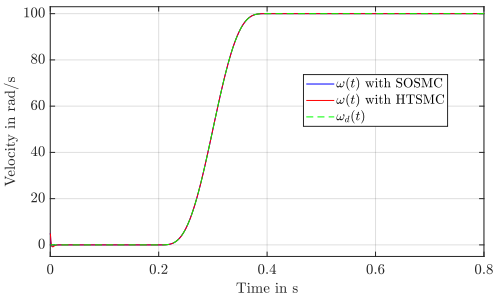

Fig. 2. Comparison of desired and simulated angular velocities using SOSMC and HTSMC.

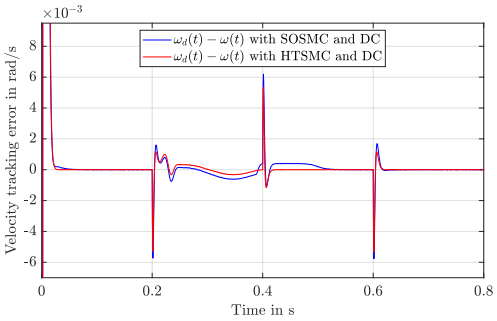

Fig. 3. Comparison of the tracking errors w.r.t. the angular velocities using SOSMC and HTSMC.

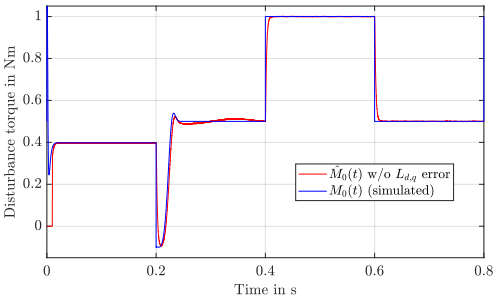

Fig. 4. Comparison of the simulated and estimated disturbance torques.

necessary control input for the case without DC is shown in Fig. 5 for the case without disturbance compensation (DC). Here, the noise level is similar for both SOSMC and HTSMC. The control inputs for an active DC can be seen in Fig. 6. To complete the investigation, simulation results are provided for the underlying inversion-based current control, see Fig. 7 and Fig. 8 The simulation results

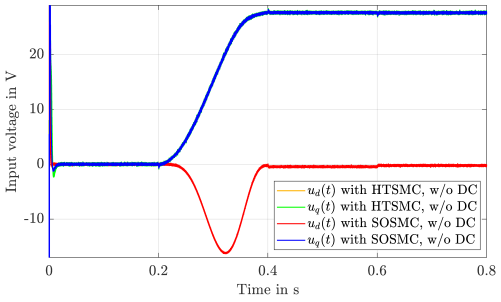

Fig. 5. Control input for the case without DC.

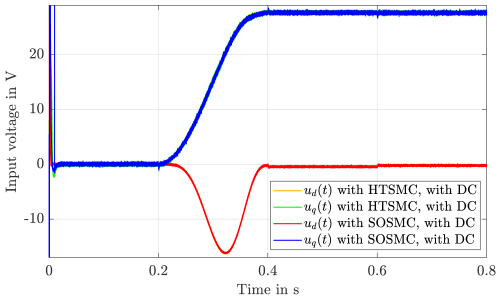

Fig. 6. Control inputs for the case with DC.

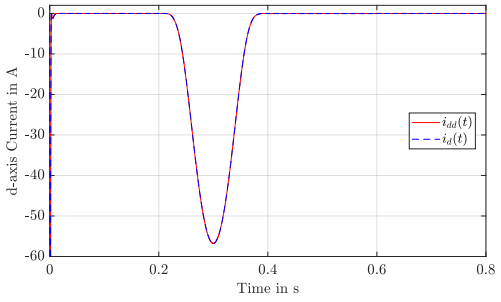

Fig. 7. Desired and simulated d-currents with SOSMC.

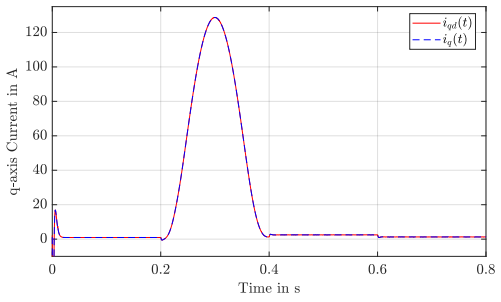

Fig. 8. Desired and simulated q-currents with SOSMC.

indicate the high tracking accuracy achieved in the inner loop.

5.2 Simulation Results With Parameter Uncertainty

The corresponding tracking errors are shown for both control approaches in Fig. 9 for the case with large deviations in the inductances. The benefits of DC become obvious because the corresponding tracking errors with an active DC are smaller than in the case without DC. Fig. 10 shows the disturbance estimation error and illustrates the high quality of the disturbance estimation by the EKF. As the comparison with the simulated disturbance shows,

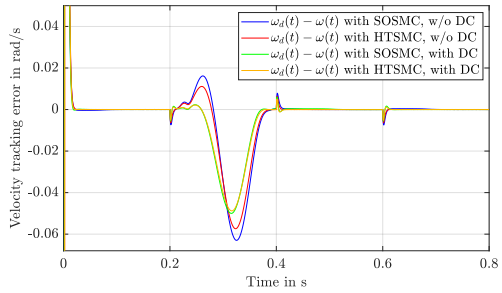

Fig. 9. Tracking error for the angular velocity for the cases with and without disturbance compensation.

nonlinear friction, an external disturbance torque and the impact of the uncertain inductances – which is relevant during tracking in the phase between 0.2 s up to 0.4 s – are significant and estimated quite well by the lumped disturbance variable. The resulting tracking error increase

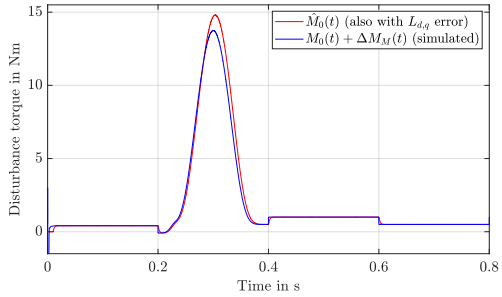

Fig. 10. Comparison of the simulated and estimated disturbance torques.

only a little as reflected by the numerical values in Table 1. This points out clearly that the proposed structure combining estimator-based disturbance compensation and second-order SMC is robust and allows for an accurate tracking despite these large uncertainties.

6. CONCLUSIONS

The paper presents a nonlinear cascaded control concept for a permanent magnetic synchronous motor (PMSM). Here, two different second-order sliding mode control approaches are compared to each other: the first one – SOSMC – includes an integrator extension of the input, whereas the other is given by a hybrid twisting sliding mode control (HTSMC). Thereby, the switching part does not affect the control inputs directly. This outer loop provides the reference currents based on an approach kwown as maximum torque per ampere (MTPA), where an accurate tracking of the reference values is achieved by an inversion-based current control. A dedicated discrete-time extended Kalman filter (EKF) estimates state variables as well as a lumped disturbance force from noisy measurements. Successful simulation results indicate that the proposed control structure consisting of a combination of disturbance compensation and second-order SMC provides a large robustness regarding parameter uncertainty and a highly accurate tracking control of the angular velocity of the PMSM.

REFERENCES

Aschemann, H., Haus, B., and Mercorelli, P. (2018). Sliding mode control and observer-based disturbance compensation for a permanent magnet linear motor. In *Proc. of the American Control Conf. (ACC)*. Milwaukee, USA.

Åström, K.J. and de Wit, C.C. (2008). Revisiting the LuGre friction model. *IEEE Control Systems*, 28(6), 101–114.

Bolognani, S., Oboe, R., and Zigliotto, M. (1999). Sensorless full-digital PMSM drive with EKF estimation of speed and rotor position. *IEEE Transactions on Industrial Electronics*, 46(1), 184–191.

Bolognani, S., Ortombina, L., Tinazzi, F., and Zigliotto, M. (2018). Model sensitivity of fundamental-frequency based position estimators for sensorless PM and reluctance synchronous motor drives. *IEEE Transactions on Industrial Electronics*, 65(1).

Friedland, B. (1996). *Advanced Control System Design*. Prentice Hall.

Khaburi, D.A. and Shahnazari, M. (2003). Parameters identification of permanent magnet synchronous machine in vector control. In *Proc. of the 10th European Conference on Power Electronics and Applications, EPE 2003*. Toulouse, France.

Levant, A. and Pridor, A. (2000). Aircraft pitch control via second order sliding technique. *AIAA Journal of Guidance, Control and Dynamics*, 23(4), 586–594.

M.A. Rahman, D.M. Vilathgamuwa, M.U. and King-Jet, T. (2003). Nonlinear control of interior permanent magnet synchronous motor. *IEEE Trans. Ind. Appl.*, 39(2), 408–416.

Mercorelli, P. (2014). An adaptive and optimized switching observer for sensorless control of an electromagnetic valve actuator in camless internal combustion engines. *Asian J. Contr.*, 16(4), 959–973.

Mercorelli, P. (2015). A two-stage sliding-mode high-gain observer to reduce uncertainties and disturbances effects for sensorless control in automotive applications. *IEEE Trans. Ind. Electron.*, 62(9), 5929–5940.

Mercorelli, P. (2017). A motion-sensorless control for intake valves in combustion engines. *IEEE Transactions on Industrial Electronics*, 64(4), 3402–3412.

Slotine, J.E. and Li, W. (1991). *Applied Nonlinear Control*. Prentice-Hall, Englewood Cliffs, NJ.

Soricellis, M.D., Rú, D.D., and Bolognani, S. (2017). A robust current control based on proportional-integral observers for permanent magnet synchronous machines. *IEEE Transactions on Industry Applications*, 54(2), 1437–1447.

Y. Shtessel, C. Edwards, L.F. and Levant, A. (2014). *Sliding Mode Control and Observation*. Springer, New York.

Zwerger, T. and Mercorelli, P. (2018). Combining an internal SMC with an external MTPA control loop for an interior PMSM. In *2018 23rd International Conference on Methods Models in Automation Robotics (MMAR)*, 674–679.

Zwerger, T. and Mercorelli, P. (2019). Combining SMC and MTPA using an EKF to estimate parameters and states of an interior PMSM. In *2019 20th International Carpathian Control Conference (ICCC)*, 1–6.